



Full Text View

[Volume 31, Issue 9 \(September 2001\)](#)

Journal of Physical Oceanography

Article: pp. 2749–2760 | [Abstract](#) | [PDF \(204K\)](#)

The Influence of Stratification on the Wind-Driven Cross-Shelf Circulation over the North Carolina Shelf*

Steven J. Lentz

Department of Physical Oceanography, Woods Hole Oceanographic Institution, Woods Hole, Massachusetts

(Manuscript received June 28, 2000, in final form February 6, 2001)

DOI: 10.1175/1520-0485(2001)031<2749:TIOSOT>2.0.CO;2

ABSTRACT

Wind-driven, cross-shelf circulation is studied using current observations spanning the 90 km wide North Carolina shelf. Most of the shelf is less than 40 m deep. Current measurements were made at five sites within 16 km of the coast from August through October or early December 1994 and at mid- and outer-shelf sites from February 1992 through February 1994. In both studies the water column was stratified in summer and often unstratified during fall and winter. The presence or absence of stratification had a profound influence on the wind-driven, cross-shelf circulation over this shallow shelf.

When the water column was stratified, the wind-driven cross-shelf circulation was consistent with a two-dimensional upwelling/downwelling response. Over the mid and outer shelf, near-surface and near-bottom cross-shelf transports had similar magnitudes but opposite directions and were approximately equal to the Ekman transports associated with the alongshelf wind stress and bottom stress, respectively. Wind-driven cross-shelf transports decreased toward the coast over a cross-shelf scale of ≈ 10 km, suggesting that upwelling and downwelling were confined near the coast during stratified conditions. Stratification may be maintained in the region of transport divergence near the coast by a balance between vertical mixing and buoyancy forcing.

When the water column was unstratified the wind-driven cross-shelf circulation at all mooring sites was substantially reduced relative to the stratified response for moderate to strong wind stresses ($|\tau^s| > 0.1 \text{ N m}^{-2}$); consistent with an Ekman depth greater than the water depth. The dependence of the cross-shelf transport on wind stress and water depth is roughly consistent with an unstratified, two-dimensional model where the eddy-viscosity profile depends on the stress and distance from the boundaries. Both observations and model results suggest that during unstratified conditions much of the divergence or convergence in the wind-driven cross-shelf transport, and hence the associated upwelling and downwelling, occurs near the shelfbreak on this shallow shelf.

Table of Contents:

- [Introduction](#)
- [Field programs and analysis](#)
- [Cross-shelf circulation](#)
- [Conclusions](#)
- [REFERENCES](#)
- [TABLES](#)
- [FIGURES](#)

Options:

- [Create Reference](#)
- [Email this Article](#)
- [Add to MyArchive](#)
- [Search AMS Glossary](#)

Search CrossRef for:

- [Articles Citing This Article](#)

Search Google Scholar for:

- [Steven J. Lentz](#)

1. Introduction

The wind-driven cross-shelf circulation is a key component of shelf dynamics and an important mechanism for cross-shelf exchange on most shelves. Yet our understanding of the wind-driven cross-shelf circulation and how it depends on stratification, bathymetry, and forcing remains poor due in part to a lack of observations.

For the simple case of a two-dimensional (no alongshelf variation) unstratified shelf forced by an alongshelf wind stress, [Ekman \(1905\)](#) showed that in deep water the steady, wind-driven transport should be perpendicular to the applied surface stress τ^s , with a magnitude $\tau^s/(\rho_o f)$ (the Ekman transport), where ρ_o is a reference density, and f is the Coriolis parameter. The wind-driven transport is confined to a boundary layer of thickness δ_E , equal to $(2A/f)^{1/2}$ for a constant eddy viscosity A ([Ekman 1905](#)) or proportional to u_*^*/f ($u_*^* = (\tau/\rho_o)^{1/2}$ is the shear velocity) for a turbulent, unstratified flow ([Csanady 1967](#); [Gill 1968](#)). For water depths h of order δ_E or less, the transport perpendicular to the applied stress is reduced until the transport is entirely downwind for water depths much less than δ_E . This occurs because the diffusive timescale to transfer momentum from the surface to the bottom, h^2/A , is less than the rotation timescale $1/f$ when h is less than δ_E . This dependence on h implies a divergence in the wind-driven cross-shelf transport between the coast ($h = 0$) and deep water ($h \gg \delta_E$). Model studies ([Ekman 1905](#); [Mitchum and Clarke 1986](#); [Lentz 1995](#)) suggest that on an unstratified shelf the cross-shelf structure of the wind-driven flow should depend primarily on the wind stress, Coriolis parameter, and the water depth. However, the details of the dependence are not known, primarily because the vertical structure of the eddy viscosity is uncertain ([Lentz 1995](#)).


Stratification inhibits vertical mixing that might allow the wind-driven cross-shelf circulation to extend into shallower water relative to an unstratified shelf. However, the stratified wind-driven response is complicated because of the feedback between stratification, vertical mixing, and the cross-shelf circulation. Recent two-dimensional model studies have begun to provide insight into wind-driven upwelling and downwelling in the presence of stratification (e.g., [de Szoeke and Richman 1984](#); [Allen et al. 1995](#); [Allen and Newberger 1996](#); [Austin 1998](#)). In these studies an upwelling or downwelling front forms and moves offshore due to the wind-driven Ekman transport. The region onshore of the front is unstratified during downwelling with essentially no cross-shelf circulation ([Allen and Newberger 1996](#)) and weakly stratified during upwelling, which allows the cross-shelf circulation to extend onshore to the coast ([Allen et al. 1995](#)).


Observational studies that evaluate models of the stratified wind-driven response on a shelf are limited and there have been no observational studies of the unstratified response. While the wind-driven flow is not always two-dimensional (e.g., [Brink et al. 1980](#)), a few studies find evidence for a two-dimensional wind-driven cross-shelf circulation on stratified shelves ([Badan-Dangon et al. 1986](#); [Lentz 1995](#); [Dever 1997](#)). But there are no studies that clearly show where the divergence in the wind-driven cross-shelf circulation occurs, what scales the divergence region has, or how the presence or absence of stratification influences the cross-shelf circulation. The importance of these questions has been emphasized in a recent model study by [Samelson \(1997\)](#), who noted the need for a better understanding of the dynamics that control the horizontal divergence in the cross-shelf circulation near the coast because the response of simple shelf models, such as coastal-trapped-wave theory, are sensitive to the prescription of the coastal boundary condition on cross-shelf velocity.

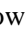
Moored current observations spanning the shallow North Carolina shelf ([section 2](#)) are used to characterize the wind-driven cross-shelf circulation and to address two related questions ([section 3](#)). First, what is the cross-shelf structure of the wind-driven, cross-shelf circulation and, in particular, where does convergence or divergence in the cross-shelf circulation occur? Second, how does the presence or absence of stratification influence the character of the wind-driven cross-shelf circulation? The moored current observations are ideal for addressing these questions because the current time series include both stratified and unstratified conditions and the measurements are concentrated near the coast, where cross-shelf variations in the flow are likely to be largest.


2. Field programs and analysis

a. Field programs

Seven mooring sites spanned the North Carolina shelf about halfway between Chesapeake Bay and Cape Hatteras, in a region where the coastline is relatively straight with an orientation of about 340°T ([Fig. 1](#) ). The water is 20 m deep 5 km offshore, increases gradually (slope 3×10^{-4}) to 40 m deep 75 km offshore, and then increases more rapidly to 100 m deep at the shelf break 90 km offshore. Thus, most of the shelf is 20 to 40 m deep. The bathymetry is rough on scales of a few

kilometers offshore of the 20-m isobath (Fig. 1 , bottom).

Current observations are from two separate field programs that were not simultaneous. Measurements were made at five sites within 16 km of the coast on the 4-m, 8-m, 13.5-m, 21-m, and 26-m isobaths from August through October or early December 1994 as part of the Coastal Ocean Processes Inner Shelf (CoOP94) study (Lentz et al. 1999). Measurements were made at two sites over the mid- (35-m isobath) and outer shelf (60-m isobath) from February 1992 through February 1994 as part of a Minerals Management Services (MMS) study of the circulation in this region (Berger et al. 1994). Instrumentation was mounted on towers at the 4-m and 8-m sites and on moorings at the other sites. Vertical spacing between current meters was 1–5 m at the five shallower sites, but only three current meters spanned the water column at the 35-m and 60-m sites (Fig. 1 ). The shallowest current meters were 4–5 m below the surface, except at the 4-m and 8-m sites. Marsh–McBirney electromagnetic current meters (EMCMs) were mounted on the 4-m and 8-m towers, vector-measuring current meters (VMCMs) on the 13-m, 21-m, and 26-m moorings, and a combination of Aanderaa, General Oceanics, and InterOcean S4 current meters on the 35-m and 60-m moorings. The EMCMs and VMCMs have estimated accuracies of 2–3 cm s⁻¹ (Guza et al. 1988; Beardsley 1987). Data return varied considerably, resulting in 2–3 month time series from CoOP94 and 15 month (35-m site) or 18 month (60-m site) time series from the MMS study.

Temperature measurements were made at roughly the same depths as the current measurements at each site. Additional temperature and conductivity measurements spanning the water column provide density time series from the 13-m, 21-m, and 26-m sites. Alongshelf arrays of bottom pressure, temperature, and conductivity instruments provide estimates of the alongshelf pressure gradient. There were five sites along the 5-m isobath with 15-km spacing and three along the 20-m isobath with 30-km spacing. Wind measurements were obtained from the end of a pier at the Army Corp of Engineers' Field Research Facility (FRF) for CoOP94 and from NDBC buoy 44014 for the MMS study (Fig. 1 ). Comparison of wind measurements in the region indicate that winds have horizontal correlation scales of 600 km and therefore are approximately uniform over the study area (Austin and Lentz 1999).

b. Processing

Instruments sampled at various rates, so a common time base was formed by block averaging the time series to hourly values centered on the hour. To focus on subtidal variability, time series were low-pass filtered to retain only periods longer than 33 hours. Biases and drifts in some of the conductivity time series were corrected by comparisons with adjacent moored conductivity time series and shipboard CTD casts taken near the moorings. Salinity and density were estimated from temperature and corrected conductivity (Fofonoff and Millard 1983).

Currents were polarized along-isobath. Principal axis orientations for the CoOP94 inner-shelf depth-averaged currents were within 5° of the coastline orientation. Therefore, the inner-shelf current and wind vector time series were rotated to a coordinate system with y alongshelf, positive toward 340°T, and x positive offshore. For the MMS sites, a coordinate system based on the principal axis was chosen with y positive toward 346°T for the 35-m site and 5°T for the 60-m site. The basic results of this study are not sensitive to small ($\sim 10^\circ$) changes in the alongshelf orientation, primarily because the depth-averaged flow, which is the major contribution to the polarized character of the flow, is removed as described below.

c. Alongshelf momentum balance

The relationship between the cross-shelf flow and the wind stress is examined using the alongshelf momentum balance integrated from the surface ($z = 0$) to a depth $z = -\delta^s$:

$$\int_{-\delta^s}^0 (v_t + uv_x + vv_y + wv_z + P_y/\rho_o) dz + fU^s = \tau^{sy}/\rho_o - \tau^y(z = -\delta^s)/\rho_o, \quad (1)$$

where u , v , and w are the cross-shelf, alongshelf, and vertical velocity components, subscripts indicate differentiation, P_y is the alongshelf pressure gradient, U^s is the cross-shelf transport between the surface and $-\delta^s$, and τ^{sy} is the alongshelf component of the wind stress. If the flow is steady, the nonlinear terms are small, there is no alongshelf pressure gradient, and the stress at $z = -\delta^s$ is small relative to the wind stress, then (1) reduces to the classical Ekman transport balance,

$$U^s = \frac{\tau^{sy}}{\rho_o f}. \quad (2)$$

A similar relationship between the near-bottom cross-shelf transport and the bottom stress, $U^b = -\tau^{by}/\rho_o f$, follows from integrating the alongshelf momentum balance from the bottom ($z = -h$) to a height δ^b above the bottom ($z = -h + \delta^b$) and making the same assumptions. The following analysis will focus on the Ekman transport balances (2) and equivalent for near-bottom transport. Estimates of the other terms in (1) are used to justify this approach. If the observed transports U^s and U^b do not equal the Ekman transports $\tau^{sy}/\rho_o f$ and $-\tau^{by}/\rho_o f$, then either the acceleration or pressure gradient terms on the left-hand side of (1) are large or the stress at $z = -\delta^s$ or $z = -h + \delta^b$ is large.

Vertical integrals are estimated using a trapezoidal rule and assuming the flow is vertically uniform between the surface (bottom) and the instrument nearest the surface (bottom). Periods when the 4-m or 8-m site was in the surf zone, defined as periods when the significant wave height was greater than three times the water depth, are excluded from the analysis.

Wind stress is estimated following [Large and Pond \(1981\)](#). Bottom stress is estimated using a linear drag law $\tau^{by}/\rho_o = r\mathbf{U}^b$, where $r = 5 \times 10^{-4} \text{ m s}^{-1}$ is a linear resistance coefficient and \mathbf{U}^b is the near-bottom alongshelf velocity. Depth-averaged momentum balances, an investigation of the barotropic tidal dynamics, and comparisons with log-profile estimates of the bottom stress at the 21-m site all suggest a linear drag law with $r = 5 \times 10^{-4} \text{ m s}^{-1}$ provides an accurate estimate of the bottom stress outside the surf zone ([Lentz et al. 1999, 2001](#)). The reference density is taken to be $\rho_o = 1023 \text{ kg m}^{-3}$ based on the moored observations, and $f = 0.9 \times 10^{-4} \text{ s}^{-1}$.

The acceleration term \mathbf{U}_t is estimated as a centered difference on the hourly current observations. The nonlinear terms in (1) cannot be estimated accurately from the observations. Rough estimates suggest that $u\mathbf{U}_x$ is not large relative to the wind stress term. Pressure gradients along the 5-m isobath are estimated from differences between pressure and density time series from sensors 15 km north and south of the mooring transect ([Lentz et al. 1999](#)). Pressure gradients along the 20-m isobath are estimated from pressure sensors 30 km north and south of the mooring transect.

The depth-averaged cross-shelf current is subtracted from the cross-shelf current at each depth before estimating U^s and U^b ([Dever 1997](#)). Subtidal, depth-averaged, cross-shelf currents from all seven mooring sites have means and standard deviations of 3 cm s^{-1} or less (offshore of the surfzone), roughly the magnitude of the uncertainty in the current measurements. Furthermore, depth-averaged cross-shelf currents are uncorrelated both with the wind stress and between mooring sites ([Lentz et al. 1999](#)). This suggests the depth-averaged cross-shelf currents are either dominated by instrument noise or associated with small-scale variability not related to the wind stress such as meandering of an alongshelf jet or eddies. Therefore, subsequent analyses focus on the depth-dependent cross-shelf circulation that, as will be shown, is related to the wind stress. This approach is consistent with a two-dimensional (cross-shelf and vertical) view of the wind-driven cross-shelf flow in which the net cross-shelf transport must be zero ([Lentz 1995; Dever 1997](#)).

To estimate U^s , δ^s is chosen to be the first zero crossing of the cross-shelf flow below the surface (after subtracting the depth-averaged flow) and to estimate U^b , δ^b is the first zero crossing above the bottom. These estimates of the boundary layer thickness are chosen rather than a mixed layer depth based on temperature or density ([Lentz 1992](#)) to provide a consistent procedure for stratified and unstratified conditions. The depths (heights) δ^s and δ^b tend to be near the middle of the water column without much variation (standard deviations 1–5 m, except at the 60-m site where the standard deviation is 9 m). Thus, the depth-dependent cross-shelf flow generally has a two-layer structure. At the 35-m and 60-m sites this may be a result of the poor vertical resolution. Thus, there is rarely a substantial interior region between the upper and lower layers, and as a consequence $U^s \approx -U^b$ (correlations range from -0.91 to -0.99). (Unless noted otherwise, correlations are significantly different from zero at the 95% confidence level with degrees of freedom based on the 1.5-day decorrelation timescale for the filtered transport estimates.) In the cross-shelf direction, standard deviations of U^s and U^b increase with distance offshore from less than $0.1 \text{ m}^2 \text{ s}^{-1}$ at the 4-m and 8-m sites to about $1 \text{ m}^2 \text{ s}^{-1}$ at the 60-m site. The cross-shelf transports U^s and U^b are correlated between mooring sites, in contrast to the total cross-shelf transport from the surface to the bottom. Correlations are typically between 0.4 and 0.6 and are not an obvious function of separation. Correlations between the 4-m site and the other sites are lower, 0.3–0.5, presumably because the transports are small relative to uncertainties at the 4-m site.

During stratified conditions, the standard deviations of surface (or bottom) mixed layer depth are about twice the standard deviations of δ^s (or δ^b), and mixed layer depths are not well correlated with δ^s or δ^b . Several factors probably contribute to the differences, including the sparser vertical coverage of current measurements relative to temperature measurements and the tendency for mixed layers to get thin when the surface or bottom stresses are small. However, during moderate to

strong stresses the mixed layer depths are similar to δ^s and δ^b . Consequently, U^s and U^b are correlated with the corresponding mixed layer transports, U^{sml} and U^{bml} . Correlations between U^s and U^{sml} or between U^b and U^{bml} range from 0.5 to 0.9 at the 13-m, 21-m, and 26-m sites. At the 4-m, 35-m, and 60-m sites, where there are only three temperature measurements spanning the water column, correlations are 0.3–0.4.

d. Stratification

Stratification is used as an indicator of whether the interior stress is small relative to the surface or bottom stress because there are not direct measurements of the stress profile. There was a large seasonal variation in stratification over the North Carolina shelf during both field programs (Berger et al. 1994; Austin 1999). There was a strong thermocline at ≈ 10 -m depth during the summer with temperature differences of as much as 15°C between the surface and bottom. During fall and winter the water column was often well mixed due to storms, surface cooling, and the shallowness of the water. Stratification also varied spatially over timescales of a few days. For example, upwelling or downwelling favorable winds during summer caused the thermocline to move offshore (Austin 1999), sometimes leaving an unstratified region near the coast. Density stratification within 15 km of shore was often dominated by salinity variability associated with the Chesapeake Bay plume, which intermittently reached the study region, primarily during downwelling (southwestward) favorable winds (Rennie et al. 1999). The plume was generally less than 10 m thick and confined within about 5 km of shore. Thus, during plume events in fall or winter, the region near the coast was stratified, while farther offshore the water was unstratified.

In the following analysis wind-driven cross-shelf circulation at each site is examined in the context of the stratification at that site. The surface-to-bottom density or temperature difference is used as a measure of whether the water at a site is stratified or unstratified. The water column is assumed to be unstratified when $\Delta\sigma_\theta < 0.3$ at the 13-m, 21-m, and 26-m sites, $|\Delta T| < 0.05^\circ\text{C}$ at the 4-m and 8-m sites, and $|\Delta T| < 0.2^\circ\text{C}$ at the 35-m and 60-m sites (Δ implies the difference between the shallowest and deepest temperature or density measurement at a site). The temperature and density cutoffs are based on the estimated in situ accuracy of the measurements.

The presence or absence of stratification may not always be a good indicator of whether the interior stress is small. For example, when stratification is present but being eroded, vertical mixing may extend throughout the water column. There may also be a balance between vertical mixing and buoyancy sources, such as the Chesapeake plume or surface heating, so that stratification is maintained in the presence of strong vertical mixing. Nevertheless, interior stresses inferred from the alongshelf momentum balance (1) suggest that the presence or absence of stratification is generally a good indicator of whether the interior stress is small compared with the surface and bottom stresses (section 3b).

3. Cross-shelf circulation




The initial focus is on the 26-m site because it is far enough offshore that there are not large changes in stratification associated with either the Chesapeake Bay plume (Rennie et al. 1999) or upwelling and downwelling of the thermocline (Austin 1999). Cross-shelf velocities during some wind events are qualitatively consistent with a two-dimensional circulation in response to upwelling or downwelling favorable winds (Figs. 2a,b). For example, a moderate southeastward (downwelling) wind stress on 19 September results in onshore flow in the upper 10 m and offshore flow in the lower 10 m of the water column (Fig. 2a). The opposite flow pattern is observed during a moderate northwestward (upwelling) wind stress on 1 October (Fig. 2b). These examples are typical of the wind-driven response when the water column is stratified. However, this simple cross-shelf flow pattern is not evident when the water column is unstratified. For example, during a strong southeastward wind stress on 15 October, the cross-shelf flow is weak (Fig. 2c), despite wind stresses that are 6–8 times larger than the previous two examples.

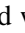
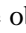
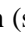


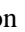
A more quantitative comparison is provided by time series of the observed cross-shelf transports U^s and U^b and the corresponding stress-driven Ekman transports $\tau^{sy}/\rho f$ and $-\tau^{by}/\rho f$ (Fig. 3). Near-surface cross-shelf transports U^s at the 26-m site are in quantitative agreement with the wind-driven Ekman transports $\tau^{sy}/\rho f$ during periods when the water column is stratified, for example, August and most of September (Fig. 3a). In contrast, $\tau^{sy}/\rho f$ is much larger than U^s during periods when the water column is unstratified, such as 4–5 September and 1–20 October. The same relationships are evident between U^b and $-\tau^{by}/\rho f$ (Fig. 3b). Shutdown of the cross-shelf circulation occurs abruptly if the water becomes unstratified during an event. For example, on 23 September 1992 the water is stratified at the 35-m site and strong winds toward the southwest (a Nor'easter) initially drive a downwelling cross-shelf circulation of $\sim 0.2 \text{ m s}^{-1}$, with onshore flow in the upper water column and offshore flow in the lower water column (Fig. 4). However, when the water column becomes unstratified on 24 September, the cross-shelf circulation abruptly shuts down, even though the alongshelf wind stress remains large. There are numerous examples in both the CoOP94 and MMS observations of similar events where the


cross-shelf circulation abruptly shuts down when the water column becomes unstratified.



Similar differences between the stratified and unstratified responses are observed at all seven mooring sites. However, the magnitude of the cross-shelf transport for a given stress varies across the shelf. The cross-shelf structure of the stress-driven cross-shelf transports during stratified and unstratified conditions is examined in the next two subsections.

a. Unstratified response

For unstratified conditions, U^s is typically onshore for downwelling (negative) winds and offshore for upwelling (positive) winds (Figs. 5a,c,e ; solid and dashed curves represent model results discussed below). However, for wind stress magnitudes greater than 0.1 N m^{-2} ($\tau^{sy}/\rho_0 f > 1.1 \text{ m}^2 \text{ s}^{-1}$), U^s is smaller than the Ekman transport (see also Fig. 3 ) and the magnitude of U^s is independent of the wind stress magnitude. Onshore transports during downwelling favorable winds are typically larger in deeper water (note change in scale of U^s for the three sites shown in Figs. 5a,c,e ). It is not known whether this is also true for upwelling because strong upwelling wind events were not observed during CoOP94. The same relationships are observed between $-\tau^{by}/\rho_0 f$ and U^b (not shown). During unstratified conditions, estimates of the \mathbf{v}_t and P_y terms in (1) are small compared with the wind stress term, suggesting that the stress at $z = -\delta^s$ (or $-h + \delta^b$) is similar in magnitude to the surface (or bottom) stress. Simple theory (Ekman 1905; Lentz 1995) suggests that there should be a substantial stress throughout the water column if the turbulent Ekman depth $\delta_E = \kappa u_* / f$ is greater than or equal to the water depth ($\kappa = 0.4$ is von Kármán's constant). For this shallow shelf ($h < 40 \text{ m}$) δ_E is greater than the water depth for wind stress magnitudes greater than $\approx 0.1 \text{ N m}^{-2}$.

The vertical structure of the eddy viscosity for a stress-driven, rotating, unstratified flow is not known (Lentz 1995). The wind-driven cross-shelf transport dependence on $\tau^{sy}/\rho_0 f$ from two-dimensional models (no alongshelf variation) using two different eddy-viscosity profiles (Fig. 6 ) is compared with the observed response (Fig. 5 ). Both eddy-viscosity profiles have a $\kappa u_* z$ dependence near the surface and bottom boundaries (z in this case is distance from the boundary). However, one of the eddy-viscosity profiles is parabolic with a maximum at middepth (solid lines, Figs. 5 and 6 ). This is the neutral (unstratified, no buoyancy forcing) profile from the Mellor–Yamada level 2.5 turbulence closure model (Mellor and Yamada 1982) implemented as part of the Princeton Ocean Model (Blumberg and Mellor 1987) as in Allen et al. (1995). The other eddy-viscosity profile decreases exponentially toward the interior when $h > \delta_E$ (dashed lines, Figs. 5 and 6 ) and is implemented in a simpler two-dimensional model (Lentz 1995). When δ_E is large compared with h , the two eddy-viscosity profiles are similar ($\tau^{sy} = 0.5 \text{ N m}^{-2}$ in Fig. 6 ). In the models, $U^s \approx \tau^{sy}/\rho_0 f$ for small wind stresses because $h > \delta_E$ (Fig. 5 ). When $h < \delta_E$, U^s is only a weak function of $\tau^{sy}/\rho_0 f$. The models reproduce the magnitude and the qualitative character of the observed relationship between $\tau^{sy}/\rho_0 f$ and U^s and between $-\tau^{by}/\rho_0 f$ and U^b (not shown). The agreement is best at the midshelf 35-m site where the cross-shelf velocities tend to be larger and there are substantially more data points.

In these simple two-dimensional models the cross-shelf transport U^s (or U^b) normalized by the Ekman transport is only a function of h/δ_E , so the model results and the observations from the various sites should collapse on a single curve (Fig. 7 ). The observations exhibit the general tendency of small transports when h/δ_E is less than 1, but there is considerable scatter. Bin averages of the normalized transport as a function of h/δ_E are more consistent with the parabolic eddy-viscosity profile than the eddy-viscosity profile that decays exponentially toward the interior. However, there is too much scatter in the observations for this comparison to be anything more than suggestive of which eddy-viscosity parameterization is most appropriate. The results suggest that careful field measurements over unstratified shelves would shed light on the appropriate form of the eddy-viscosity profile.

Several factors undoubtedly contribute to the scatter in the observations (Figs. 5 and 7 ). Uncertainty in the transports is often large because the corresponding cross-shelf velocities are small compared with the accuracy of the current measurements. The vertical structure of the flow is not well resolved, particularly at the 35-m and 60-m sites. Temperature (4-m, 8-m, 35-m, and 60-m sites) is not always a good proxy for density, especially near the coast where there are large salinity variations associated with the Chesapeake Bay plume and near the shelf break where there are large salinity variations associated with the shelfbreak front. This may account for the relatively large transports that appear to be consistent with stratified flow conditions at the 8-m site (cf. Figs. 5a and 5b ). Finally, the models assume neutral conditions, while for the inner-shelf observations unstratified conditions occurred primarily during strong surface cooling, which would force convection, increasing the vertical mixing relative to the neutral case.

The observations and model results indicate that during unstratified conditions in fall and winter the wind-driven cross-shelf transport is reduced relative to the Ekman transport across the entire North Carolina shelf for wind stress magnitudes larger than $\sim 0.1 \text{ N m}^{-2}$. This suggests that strong wind-forcing may not be a very effective mechanism for cross-shelf movement of organisms, nutrients, or sediment during the fall and winter. The results also suggest that most of the transport divergence in the wind-driven cross-shelf flow occurs near the shelfbreak during strong winds when the shelf is unstratified. These cross-shelf transport divergences imply upwelling or downwelling (because of continuity) if the flow is roughly two-dimensional, that is, there are not significant depth-dependent alongshelf transport divergences. The region of divergence in the wind-driven cross-shelf transport is often referred to as the “inner shelf” (Lentz 1994), and in coastal-trapped-wave theory the coastal boundary condition is normally applied offshore of this region (Mitchum and Clarke 1986). Thus, during moderate to strong wind forcing in fall and winter, almost the entire southern Middle Atlantic Bight shelf is an “inner shelf” and hence is onshore of the coastal boundary condition in classical coastal-trapped-wave theory.

b. Stratified response

For stratified conditions there is a linear relationship between $\tau^y/\rho f$ and U at all sites (Figs. 5b,d,f; Table 1). The largest stresses and transports, $\sim -3 \text{ m}^2 \text{ s}^{-1}$ at the 35-m site (Fig. 5f), occurred during a summer hurricane that reduced but did not destroy the stratification. A linear regression of the form $U = a(\tau^y/\rho f) + b$ yields a slope a of approximately 1.0 for the mid- and outer-shelf (25 m, 35 m, and 60 m) sites indicating that the cross-shelf transport is, on average, equal to the wind or bottom stress-driven Ekman transport (Table 1 and Fig. 8). (The regression slopes at the 60-m site are greater than 1.0, probably because δ^s and δ^b are overestimated using only three current meters.) The observation that $U^s \approx \tau^s/\rho f$ and $U^b \approx -\tau^b/\rho f$ at the mid- and outer-shelf sites is consistent with stratification inhibiting turbulent mixing in the interior so the interior stress is small compared with the surface or bottom stress. Onshore of the 26-m site the regression slopes decrease toward zero at the coast, indicating that for stratified flow there is a divergence of the stress-driven transport within about 10 km of the coast. Correlations are generally significant at the 95% level, but not high in some cases (Table 1). Intercepts are zero to the accuracy of the estimates, indicating that cross-shelf transports in the upper and lower layers are small in the absence of a surface or bottom stress.

The increase in the regression coefficient a between U and $\tau^y/\rho f$ within 10 km of the coast is consistent with the increase in the standard deviation of U near the coast. However, the standard deviation of U continues to increase with distance offshore out to the 60-m site, while the regression slope is approximately constant over the middle and outer shelf. This suggests that there are baroclinic motions contributing to U^s and U^b over the middle and outer shelf that are not wind driven.

Inclusion of the \mathbf{v}_t and P_y terms in (1) as part of the forcing does not change the cross-shelf structure of the slope a in Fig. 8. Rough estimates of the $u\mathbf{v}_x$ term suggest that, while \mathbf{v}_x can be the same magnitude as f in shallow water, this term is not large compared with the wind stress term and does not account for the reduction in the regression coefficient within 10 km of the coast. These results and the reduction in the cross-shelf transport near the coast imply that the stress at $z = -\delta^s$ or $-h + \delta^b$ is comparable to the surface or bottom stress. For evidence of the potential for vertical mixing that would be associated with the middepth stresses, bulk estimates of the Richardson number, $\text{Ri} = (-g\Delta\rho/\rho_0 \Delta z)/(\Delta u/\Delta z)^2$ based on density $\Delta\rho$ and velocity Δu differences through the water column (Δz is the separation between the top and bottom instruments), were computed at the three sites for which there are density time series (13 m, 21 m, and 26 m). Small values of Ri , near a critical value of 1 (or 0.25), are far more common at the 13-m and 21-m sites than at the 26-m site (Fig. 9). For example, in August Ri was rarely less than 2 at the 26-m site yet was often less than 1 at the 13-m site. Additionally, at the 26-m site Ri is only less than 1 when $\Delta\sigma_\theta \approx 0$. In general, there is not as clear a correspondence between $\Delta\sigma_\theta$ and Ri at the 13-m site as at the 26-m site. At the 13-m (and 21-m) site there are often times when there is substantial stratification and Ri is one or less, for example, the first week in September. In many cases these low Ri events at the 13-m site are associated with the Chesapeake plume, suggesting the plume is providing a source of buoyancy that is maintaining the stratification in the presence of vertical mixing. Surface heating may also be important in this regard. Thus, these observations suggest that within 10 km of the coast the water is shallow enough that wind-driven vertical mixing can extend through the water column and balance buoyancy sources such as the Chesapeake Bay plume or surface heating. The width of the divergence in the cross-shelf velocity may also be related to the thermocline displacements associated with upwelling and downwelling. The thermocline was typically displaced more than 5 km offshore (beyond the 20-m site) and less than 16 km offshore (26-m site) during moderate to strong upwelling or downwelling favorable winds. It remains unclear what sets the cross-shelf scale of the divergence in the wind-driven cross-shelf circulation when the water is stratified.

4. Conclusions

Observations from seven current meter mooring sites spanning the North Carolina shelf indicate that the presence or

absence of stratification has a profound influence on the magnitude and cross-shelf structure of the wind-driven cross-shelf circulation.

When the water column is unstratified, the observed near-surface and near-bottom cross-shelf transports are smaller than the Ekman transports ($\tau^y/\rho g$) for moderate to strong wind or bottom stresses ($|\tau^y| > 0.1 \text{ N m}^{-2}$), consistent with the Ekman depth δ_E being greater than or equal to the water depth (typically less than 40 m). This suggests that during moderate to strong wind stress events much of the Ekman transport divergence and the associated upwelling and downwelling occur near the shelf break when the shelf is unstratified. Simple, two-dimensional models with eddy-viscosity profiles that increase linearly away from the boundaries reproduce the basic relationship between the observed cross-shelf transports and the wind stress or bottom stress.

When the water column is stratified, the observed near-surface and near-bottom cross-shelf transports are approximately equal to stress-driven Ekman transports over the mid and outer shelf. The cross-shelf transports decrease toward zero near the coast over a cross-shelf scale of about 10 km, suggesting that upwelling and downwelling occur within 10 km of the coast during stratified conditions. Estimates of the Richardson number, from the moored current and density time series, are often less than one in the region of cross-shelf transport divergence, but not farther offshore during stratified conditions. This, combined with the observation that the acceleration and alongshelf pressure gradient terms in the alongshelf momentum balance are small, suggests that vertical mixing may result in large stresses throughout the water column even though the water is stratified. Buoyancy forcing from the Chesapeake Bay plume and surface heating may maintain the stratification in the presence of the inferred vertical mixing. A major shortcoming of this analysis is that interior stresses are inferred rather than measured. Direct measurements of the stress profile throughout the water column would greatly facilitate interpretation of the dynamics associated with the wind-driven cross-shelf circulation.

Acknowledgments

The 4- and 8-m current data were provided by S. Elgar, R. T. Guza, and T. H. C. Herbers, funded by the Office of Naval Research (Coastal Dynamics) and the National Science Foundation (Coop). The current data from the Minerals Management Services study were provided by Jim Churchill. Some of the wind and wave data used were acquired, processed, and archived by the staff at the Field Research Facility of the U.S. Army Engineer Waterways Experiment Stations's Coastal Engineering Research Center. Permission to use each of these datasets and the effort involved in acquiring data of this quality are greatly appreciated. I appreciate comments on earlier drafts of this manuscript by D. Chapman, K. Brink, R. T. Guza, S. Elgar, and two anonymous reviewers. Financial support for S. Lentz was provided by the Ocean Sciences Division of the National Science Foundation as part of the Coastal Ocean Processes program under Grants OCE-9221615 and OCE-9633025.

REFERENCES

- Allen J. S., and P. A. Newberger, 1996: Downwelling circulation on the Oregon continental shelf. Part I: Response to idealized forcing. *J. Phys. Oceanogr.*, **26**, 2011–2035. [Find this article online](#)
- Allen J. S., P. A. Newberger, and J. Federiuk, 1995: Upwelling circulation on the Oregon continental shelf. Part I: Response to idealized forcing. *J. Phys. Oceanogr.*, **25**, 1843–1866. [Find this article online](#)
- Austin J. A., 1998: Wind-driven circulation on a shallow, stratified shelf. Ph.D. thesis, Massachusetts Institute of Technology and Woods Hole Oceanographic Institution Joint Program, Woods Hole, MA, 243 pp.
- Austin J. A., 1999: The role of the alongshore wind stress in the heat budget of the North Carolina inner shelf. *J. Geophys. Res.*, **104**, 18187–18203. [Find this article online](#)
- Austin J. A., and S. J. Lentz, 1999: The relationship between synoptic weather systems and meteorological forcing on the North Carolina inner shelf. *J. Geophys. Res.*, **104**, 18159–18186. [Find this article online](#)
- Badan-Dangon A., K. H. Brink, and R. L. Smith, 1986: On the dynamical structure of the midshelf water column off northwest Africa. *Contin. Shelf Res.*, **5**, 629–644. [Find this article online](#)
- Beardsley R. C., 1987: A comparison of the vector-averaging R current meter and new Edgerton, Germeshausen, and Grier, Inc., vector-measuring current meter on a surface mooring in CODE 1. *J. Geophys. Res.*, **92**, 1845–1860. [Find this article online](#)
- Berger T. J., W. C. Boicourt, J. H. Churchill, P. Hamilton, R. J. Wayland, and D. R. Watts, 1994: A physical oceanographic field program offshore of North Carolina. Tech. Rep. MMS 94, Science Applications International Corporation, 463 pp.

Blumberg A. F., and G. L. Mellor, 1987: A description of a three-dimensional coastal ocean circulation model. *Three Dimensional Coastal Ocean Models*, N. Heaps, Ed., Coastal and Estuarine Science Series, Vol. 4, Amer. Geophys. Union, 1–16.

Brink K. H., D. Halpern, and R. L. Smith, 1980: Circulation in the Peruvian upwelling system near 15°S. *J. Geophys. Res.*, **85**, 4036–4048. [Find this article online](#)

Csanady G. T., 1967: On the “Resistance Law” of a turbulent Ekman layer. *J. Atmos. Sci.*, **24**, 467–471. [Find this article online](#)

de Szoeke R. A., and J. Richman, 1984: On wind-driven mixed layers with strong horizontal gradients—A theory with application to coastal upwelling. *J. Phys. Oceanogr.*, **14**, 364–377. [Find this article online](#)

Dever E. P., 1997: Wind-forced cross-shelf circulation on the northern California shelf. *J. Phys. Oceanogr.*, **27**, 1566–1580. [Find this article online](#)

Ekman V. W., 1905: On the influence of the earth's rotation on ocean currents. *Ark. Mat. Astron. Fys.*, **2**, 1–53.

Fofonoff N. P., and R. C. Millard Jr., 1983: Algorithms for computation of fundamental properties of seawater. UNESCO Tech. Paper in Marine Science 44, 53 pp.

Gill A. E., 1968: Similarity theory and geostrophic adjustment. *Quart. J. Roy. Meteor. Soc.*, **94**, 581–585. [Find this article online](#)

Guza R. T., M. C. Clifton, and F. Rezvani, 1988: Field intercomparisons of electromagnetic current meters. *J. Geophys. Res.*, **93**, 9302–9314. [Find this article online](#)

Large W. G., and S. Pond, 1981: Open ocean momentum flux measurements in moderate to strong winds. *J. Phys. Oceanogr.*, **11**, 324–336. [Find this article online](#)

Lentz S. J., 1992: The surface boundary layer in coastal upwelling regions. *J. Phys. Oceanogr.*, **22**, 1517–1539. [Find this article online](#)

Lentz S. J., 1994: Current dynamics over the northern California inner shelf. *J. Phys. Oceanogr.*, **24**, 2461–2478. [Find this article online](#)

Lentz S. J., 1995: Sensitivity of the inner-shelf circulation to the eddy-viscosity profile. *J. Phys. Oceanogr.*, **25**, 19–28. [Find this article online](#)

Lentz S. J., R. T. Guza, S. Elgar, F. Feddersen, and T. H. C. Herbers, 1999: Momentum balances on the North Carolina inner shelf. *J. Geophys. Res.*, **104**, 18205–18226. [Find this article online](#)

Lentz S. J., M. Carr, and T. H. C. Herbers, 2001: Barotropic tides on the North Carolina shelf. *J. Phys. Oceanogr.*, **31**, 1843–1859.

Mellor G. L., and T. Yamada, 1982: Development of a turbulence closure model for geophysical fluid problems. *Rev. Geophys. Space Phys.*, **20**, 851–875. [Find this article online](#)

Mitchum G. T., and A. J. Clarke, 1986: The frictional nearshore response to forcing by synoptic scale winds. *J. Phys. Oceanogr.*, **16**, 934–946. [Find this article online](#)

Rennie S., J. L. Largier, and S. J. Lentz, 1999: Observations of low-salinity coastal current pulses downstream of Chesapeake Bay. *J. Geophys. Res.*, **104**, 18227–18240. [Find this article online](#)

Samelson R. M., 1997: Coastal boundary conditions and the baroclinic structure of wind-driven continental shelf currents. *J. Phys. Oceanogr.*, **27**, 2645–2662. [Find this article online](#)

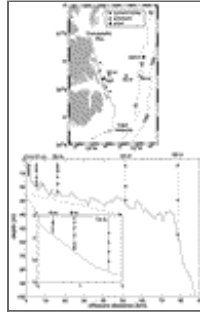
Tables

TABLE 1. Results of a linear regression analysis of the form $U = a(\tau^y/\rho_f) + b$ using daily values when the water column is stratified at each site. Water depth h , offshore distance x , number of days in analysis, correlations, and 95% confidence intervals for a and b are included. Units are $\text{m}^2 \text{s}^{-1}$ for b . Correlations not significantly different from zero at the 95% confidence level are noted with an asterisk

h (m)	x (km)	Days	Near-surface transport			Near-bottom transport		
			Intercept b	Slope a	Correlation	Intercept b	Slope a	Correlation
4	0.4	29	0.01 ± 0.01	0.08 ± 0.09	0.11*	0.00 ± 0.01	-0.08 ± 0.03	-0.67
8	0.9	33	-0.03 ± 0.02	0.21 ± 0.06	0.61	0.01 ± 0.03	-0.22 ± 0.11	-0.61
13	1.6	59	0.03 ± 0.04	0.34 ± 0.15	0.37	-0.03 ± 0.04	-0.28 ± 0.09	-0.66
21	5.4	44	0.01 ± 0.12	0.69 ± 0.66	0.39*	-0.05 ± 0.12	-0.37 ± 0.46	-0.41
28	16.4	73	0.05 ± 0.10	0.87 ± 0.20	0.74	-0.02 ± 0.10	-0.91 ± 0.20	-0.75
35	50.1	320	-0.02 ± 0.07	0.98 ± 0.10	0.74	-0.03 ± 0.07	-0.95 ± 0.10	-0.75
60	77.1	425	-0.08 ± 0.10	1.16 ± 0.12	0.71	-0.06 ± 0.16	-1.37 ± 0.34	-0.42

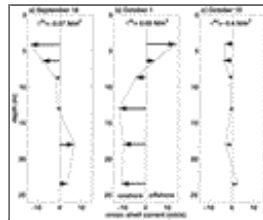
Click on thumbnail for full-sized image.

Figures



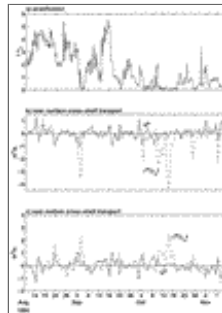
[Click on thumbnail for full-sized image.](#)

FIG. 1. Map showing study area and current meter mooring, bottom pressure, and wind measurement sites (top). There are four current meter sites onshore of the 26-m site. Wind measurements were made at the Field Research Facility pier and NDBC buoy 44014. Cross-shelf section showing bathymetry and locations of current meters (bottom). Inset is an expanded view of the region within 2 km of the coast



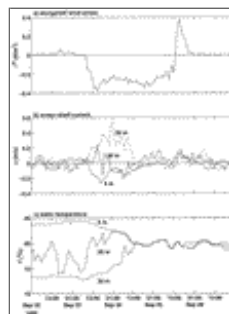
[Click on thumbnail for full-sized image.](#)

FIG. 2. Examples of cross-shelf velocity profiles at the 26-m site when the water is stratified [(a) 19 Sep, downwelling wind; (b) 1 Oct, upwelling wind] and unstratified [(c) 15 Oct, downwelling wind]. Current profiles are from low-pass filtered time series (33-h cutoff to suppress tidal flows) and they include the depth-averaged current. Positive currents are offshore



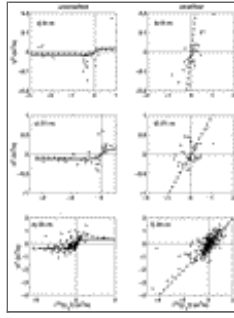
[Click on thumbnail for full-sized image.](#)

FIG. 3. Time series from the 26-m site of (a) the density difference through the water column $\Delta\sigma_\theta$; (b) the observed, near-surface, cross-shelf transport U^s (dashed) and the wind-driven Ekman transport $\tau^{sy}/(\rho g f)$; and (c) the observed, near-bottom, cross-shelf transport U^b (dashed) and the bottom-stress-driven Ekman transport $-\tau^{by}/(\rho g f)$. Positive transports are offshore. The observed transport tends to equal the Ekman transport when the water column is stratified, but the Ekman transport is much larger than the observed transport when the water column is unstratified



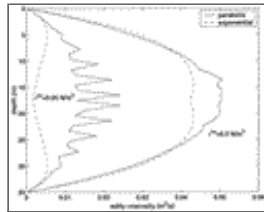
[Click on thumbnail for full-sized image.](#)

FIG. 4. Time series from the 35-m site of (a) alongshelf wind stress, (b) cross-shelf current (including depth-averaged current), and (c) temperature during an event in late Sep 1992 showing the sudden shutdown of the cross-shelf circulation when the water column becomes unstratified. During the first day of this downwelling event the flow is onshore at 5-m depth and offshore at 30-m depth. Detided, unfiltered hourly values are shown to indicate the abruptness of the shutdown



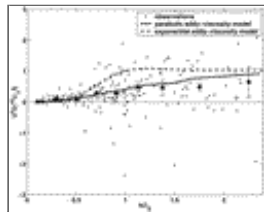
Click on thumbnail for full-sized image.

FIG. 5. Daily values of U^s as a function of $\tau^{sy}/(\rho_o f)$ when the water column is [(a), (c), (e)] unstratified and [(b), (d), (f)] stratified from the 8-m, 21-m, and 35-m sites. For unstratified panels two-dimensional model results are also shown for parabolic (solid line) and exponential (dashed line) eddy-viscosity profiles (see Fig. 6 for examples). For stratified panels dashed line is $U^s = \tau^{sy}/(\rho_o f)$. Scales for $\tau^{sy}/(\rho_o f)$ vary for each panel and scales for U^s vary for each site



Click on thumbnail for full-sized image.

FIG. 6. Examples of parabolic (solid line) and exponential (dashed line) eddy-viscosity profiles used in unstratified, two-dimensional model runs. The parabolic profiles are from the Mellor–Yamada 2.5 closure model and have a maximum at mid depth, while the exponential profile decreases to a local minimum at mid depth (for weak stresses). For large stresses or shallow water the two eddy-viscosity profiles are similar



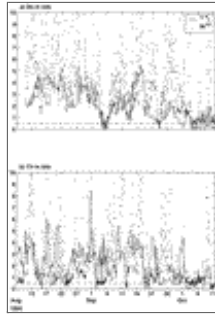
Click on thumbnail for full-sized image.

FIG. 7. Daily values of normalized cross-shelf transport $U^s/(\tau^{sy}/\rho_o f)$ as a function of normalized water depth h/δ_E when the water is unstratified (small circles) and averages binned by normalized depth (large circles). The Ekman depth $\delta_E = \kappa u_* / f$, where $\kappa = 0.4$ is von Kármán's constant, $u_* = (\tau^{sy}/\rho_o)^{1/2}$, and f is the Coriolis parameter. Results from two-dimensional models utilizing parabolic (solid line) and exponential (dashed line) eddy-viscosity profiles (see Fig. 6 for examples) are also shown. Error bars on bin-averaged observations are the standard error of the mean (standard deviation for each bin divided by the square root of the number of daily values, typically 16–25). To reduce the scatter only observations for which $|\tau^{sy}/\rho_o f| > 0.2 \text{ m s}^{-2}$ are included in the analysis. Four observations with $5 > |U^s/(\tau^{sy}/\rho_o f)| > 3$ are included in the analysis but not shown for clarity



Click on thumbnail for full-sized image.

FIG. 8. Slope a from a linear regression of the form $U = a(\tau^y/\rho_o f) + b$ as a function of offshore distance during stratified conditions for (a) near-surface and (b) near-bottom transports. Dashed line indicates $a = \pm 1$; note the decrease in a within 10 km of the coast. Intercepts, slopes, and correlations are listed in [Table 1](#)



Click on thumbnail for full-sized image.

FIG. 9. Time series of the density difference through the water column $\Delta\sigma_\theta$ and $(\text{Ri})^{1/2}$ for the (a) 26-m and (b) 13-m sites; Ri is a bulk estimate of the Richardson number based on density and velocity differences through the water column. Dashed line indicates $\text{Ri} = 0.25$

* Woods Hole Oceanographic Institution Contribution Number 10290.

Corresponding author address: Dr. Steven J. Lentz, Dept. of Physical Oceanography, Woods Hole Oceanographic Institution, Woods Hole, MA 02543. E-mail: slentz@whoi.edu

top ▲



© 2008 American Meteorological Society [Privacy Policy and Disclaimer](#)
Headquarters: 45 Beacon Street Boston, MA 02108-3693
DC Office: 1120 G Street, NW, Suite 800 Washington DC, 20005-3826
amsinfo@ametsoc.org Phone: 617-227-2425 Fax: 617-742-8718
[Allen Press, Inc.](#) assists in the online publication of AMS journals.